Sādhanā (2020)45:180
https://doi.org/10.1007/s12046-020-01412-3

Operator based finite element modelling of viscoelastic cracked propeller shaft: a comparative study

KRISHANU GANGULY, RAHUL RANJEET and HARAPRASAD ROY*

Department of Mechanical Engineering, National Institute of Technology, Rourkela 769008, India
e-mail: krishanuganguly5@gmail.com; rahulrohit519@gmail.com; hroy77@rediffmail.com

MS received 4 June 2019; revised 26 May 2020; accepted 11 June 2020

Abstract. The present study focuses on to explore the dynamic analysis of a viscoelastic propeller-shaft system with transverse breathing crack supported by journal bearings. Finite element modelling of the shaft continuum is done considering the Euler-Bernoulli beam theory. Operator based constitutive relationship is applied to incorporate material damping of the rotor and higher-order equations of motion are established. Accurate time-dependent functions are used to formulate cracked element stiffness matrix and augmented to the overall stiffness matrix of the entire system. Eigen analysis is performed after converting the higher-order equation into the first-order form. A Comparative study is demonstrated based on different dynamic parameters like whirl frequency, modal damping factor and stability limit of spin speed. Further, the variation of stability limit of spin speed and natural frequency is also studied based on the parameters such as crack depth and its location along different section of the propeller shaft.

Keywords. Viscoelastic propeller shaft; breathing crack; operator based approach; finite element model; eigen analysis.

1. Introduction

Rotor Dynamics mainly focuses on studying the vibrations in the rotor system as well as control strategy. Various types of speed-dependent forces are produced during shaft rotation which includes gyroscopic, rotating damping and bearing damping forces [1]. The modelling of these forces results to an asymmetric system [2]. Internal material damping of viscoelastic rotors produces a speed-dependent tangential rotating damping force and tends to disturb the rotor-shaft-bearing system. Thus for proper dynamic study of viscoelastic rotors, modelling should include appropriate procedures to take the internal damping into account. The time-domain representation of viscoelastic nature is explained by using the rheological model, which is a combination of linear springs and dashpots where the spring acts for elastic nature and the dashpot acts for viscous nature. Various arrangements of springs and dashpots give different rheological models of viscoelastic materials such as Kelvin –Voigt model, Maxwell model and Zener model. Bland [3]; Christensen [4]; Shames and Cozzarelli [5] and many others used different rheological models for linear viscoelastic semi-solid. Further, the modulus operator was established using different rheological models and several research works were carried out to perform dynamic analysis of viscoelastic rotor shafts [6, 7].

In recent years, studying the dynamic modelling of a cracked rotor has appeared with great and immense advancement. Manufacturing defects in the end product or cyclic loading are the main reasons for the production of fatigue cracks, which may cause catastrophic failures. Many research papers were authored for identifying crack shaft, and examination was carried out to explore the impacts of various crack parameters like depth of the crack, location of crack, loading condition and rotational speed. Apart from these parameters, one of the most significant factors is the type of crack that affects the dynamic modelling. Though there exist several types of crack, the breathing crack is considered to be critical for rotating structures. Different approaches were developed by many researchers to model a rotor shaft with a crack exhibiting breathing modelling i.e., opening and closing tendency of the crack [8, 9]. Sinou and Lees [10] modeled a rotor shaft with breathing transverse crack using an alternate frequency-/time-domain approach and conferred changes in modal properties and dynamic response. The authors Georgantzinos and Anifantis [11] discussed the breathing crack mechanism of a rotating shaft considering quasi-static approximation and refined nonlinear contact-finite element procedure. Soon, in order to significantly show the effect of opening and closing mechanism of the crack during rotation, Al-Shudeifat and Butcher [12] successfully represented new breathing functions in terms of a time-dependent area moment of inertia and studied its

*For correspondence
Published online: 15 July 2020

incorporation through orbital responses. Further considering the effect of crack parameters such as crack orientation and the number of cracks, Han and Chu [13] performed the analysis over a rotor-bearing system containing double breathing transverse cracks. Dynamic instability of the double cracked rotor gave some extraordinary features that vary from a single cracked rotor system. Guo *et al* [14, 15] used Floquet theory as well as empirical mode decomposition method to detect crack propagation and study its effect on the stability of the damped rotor system. In another monograph, Peng *et al* [16] used the numerical Floquet method for studying the stability of periodic time-dependent Jeffcott rotor containing transverse breathing crack. Most recently, Mobarak *et al* [17] generated an analytical model of a breathing crack rotor shaft system coupling the effects of unbalance force, rotor weight as well as its physical and dimensional properties. Wang *et al* [18] discussed the stability limits of spin speed of an anisotropic rotor-shaft system mounted on journal bearings containing a transverse breathing crack.

Within the same range of time, a broad spectrum of literature has been found which provides an insight into the non-linear effect of breathing crack. In this direction authors like Sinou and Lees [19] used truncated Fourier series and harmonic balance method to include the varying stiffness of the shaft due to the breathing effect of the crack. Truncated time-varying cosine series was utilized by Chen and Dai [20] for accounting the opening and closing effect of the crack and studied the nonlinear dynamics of a cracked rotor system mounted on viscoelastic supports. A finite element 3D model of cracked shaft was formulated by Bachschmid *et al* [21] and the non-linear modelling through an approximated approach was studied. Further, a more realistic variation in the stiffness matrix of a rotating shaft with a breathing crack was represented by Amer and Nguyen [22] by locating a non-linear spring at the cracked transverse section position. Chen [23] applied the finite element method to investigate the non-linear dynamic characteristics of slant breathing crack in a flexible rotor shaft system mounted on bearings exhibiting linear/non-linear forces.

Although research works related to the cracked rotor are abundant, the analyses of cracked rotor considering realistic systems are very few. Further, the modelling of a shaft with all asymmetric effects is also important for predicting proper dynamic patterns. In this study, a finite element model of a viscoelastic propeller shaft supported on journal bearings is developed. Single transverse breathing crack is introduced over the shaft continuum using accurate breathing functions. The obtained time-dependent stiffness matrix of the cracked element is assembled with the stiffness matrix of the intact elements and the global stiffness matrix is generated. The modulus operator of the three-element model is employed to tackle the damping property of the viscoelastic shaft and the higher-order equation of motion is derived. This finite element formulation of the complex propeller shaft includes various types of asymmetries like gyroscopic, internal damping and journal bearing effect. With the inclusion of crack, the formulation also becomes non-axisymmetric. Further, the first-order equation of motion is derived from the higher-order equation and eigen analysis is carried out. Dynamic characteristics of the internally damped cracked propeller shaft are studied based on different conventional parameters such as decay rate plot, Campbell diagram, modal damping factor and stability limit of spin speed.

2. Mathematical modelling

2.1 *Breathing crack formulation*

The breathing mechanism happens in the cracked rotor when the shaft is subjected to high radial force and the transverse thickness of crack is very little along the axial direction. A methodology for computing the exact breathing mechanism of breathing cracked rotor is presented in this paper after considering linear stress/strain dispersion in the crack area. The time-dependent cracked stiffness matrix is addressed here to estimate the breathing mechanism and linked to the linearly time-domain finite element equation.

The rotor cross-section of an area A with a crack segment area A_c is shown in figure 1a), where the crack portion is marked by hashed line. Figure 1a) shows the initial position ($t = 0$) of the crack surface and assumed that its edge is perpendicular to the vertical axis. The coordinate axis passing through the centre of the whole cross-section (O) is indicated by the lower case whereas the upper case is used for the coordinate axis passing through the centroid of the uncracked portion (C). The symbol tilde ($\sim$) is applied for the rotating frame of reference. Figure 1b) represents the shaft location for $t > 0$, where the crack surface makes an angle Ωt with the negative Z-axis. The distance OC is written as c, and it is changing with time during rotation.

For crack depth h, the angle made by the crack segment at the centre is θ. As the crack line is symmetric about the vertical axis, the angle is, $\theta = 2\cos^{-1}\left(\frac{r-h}{r}\right)$. The total subtended area by this angle is $\left(\frac{\theta}{2\pi}\right)\pi r^2$. The expression of the cross-sectional area of the uncracked segment ($A^{'}$) under full crack open condition is given by,

$$A^{'} = A - A_c = \left(1 - \frac{\theta}{2\pi}\right)\pi r^2 + (r-h)r\sin\left(\frac{\theta}{2}\right) \qquad (1)$$

During rotation, the crack portion above the neutral axis is subjected to compressive stress. Hence the crack starts to close at θ_1 and crack turns into fully closed state at θ_2. Where θ_1 is calculated from similar ΔCOE and ΔCFD in Figure 1b while θ_2 is calculated from ΔBCDin figure 1c) given as (Al-Shudeifat and Butcher [12]),

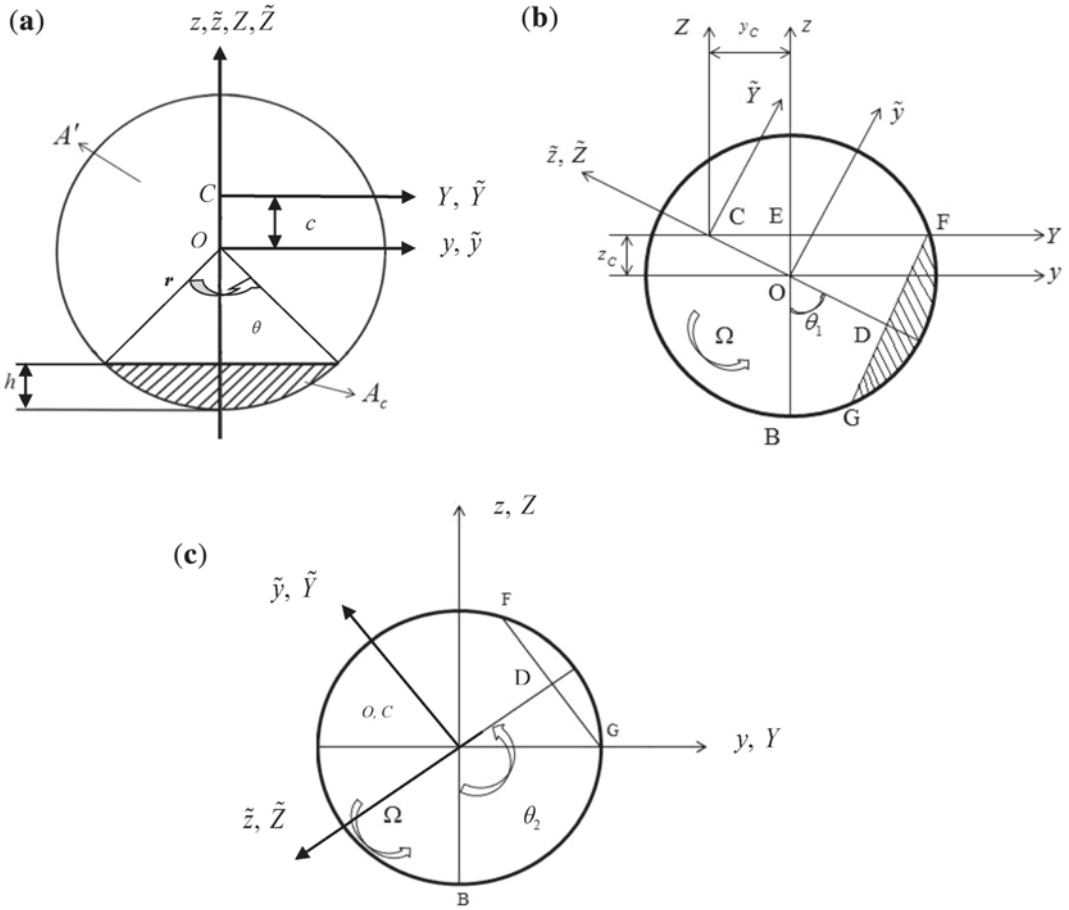

Figure 1. Different orientation of cracked element rotor cross-section a) At rest, b) When the crack starts to close and c) When the crack becomes full close.

$$\theta_1 = \tan^{-1}\left(\frac{c+(r-h)}{\sqrt{h(2r-h)}}\right), \quad \theta_2 = \frac{\pi}{2} + \cos^{-1}\left(\frac{r-h}{r}\right) \tag{2}$$

where, $c = \frac{2r^2}{3A'}(h(2r-h))^{\frac{3}{2}}$

Once the crack portion starts to close, the time-varying area of the closed crack segment is $A''(t)$. Thus at any instant of time, the uncracked portion area is given by,

$$A_o(t) = A' + A''(t) \tag{3}$$

The area moment of inertia $I_y^{A'}$, $I_z^{A'}$ of A' about fixed y and z-axis for $t = 0$ respectively is calculated as

$$I_y^{A'} = I - I_y^{A_c} \tag{4a}$$

$$I_z^{A'} = I - I_z^{A_c} \tag{4b}$$

where, $I = \frac{\pi r^4}{4}$ is the moment of inertia of whole cross-section. While area moment of inertia of the crack segment $I_y^{A_c}$ and $I_z^{A_c}$ are given as

$$I_y^{A_c} = \frac{\pi r^4}{8} - \frac{1}{4}\left(r^4 \sin^{-1}\left(\frac{r-h}{r}\right) - \left((r-h)\sqrt{h(2r-h)}\left(2rh - r^2 - h^2\right)\right)\right) \tag{5a}$$

$$I_z^{A_c} = \frac{1}{12}\left(r^4 \sin^{-1}\left(\frac{1}{r}\sqrt{h(2r-h)}\right) - (r-h)\left(3r^2 - 28hr + 14h^2\right)\sqrt{h(2r-h)}\right) \tag{5b}$$

when the shaft starts to rotate at time $t \geq 0$, the area moment of inertia of the section A' about y and z is given by Pilkey [24],

$$I_y^{A'}(t) = \frac{I_y^{A'} + I_z^{A'}}{2} + \frac{I_y^{A'} - I_z^{A'}}{2}\cos(2\Omega t) \tag{6a}$$

$$I_z^{A'}(t) = \frac{I_y^{A'} + I_z^{A'}}{2} - \frac{I_y^{A'} - I_z^{A'}}{2}\cos(2\Omega t) \tag{6b}$$

Considering total time-dependent area $A_0(t)$, the area moment of inertia about y and $z$axes is given by,

$$I_y^{A_0}(t) = I_y^{A'}(t) + I_y^{A''}(t) \tag{7a}$$

$$I_z^{A_0}(t) = I_z^{A'}(t) + I_z^{A''}(t) \tag{7b}$$

where $I_y^{A''}$ and $I_z^{A''}$ are time-dependent area moment of inertia of $A''(t)$ about y and z axes respectively.

Further, following equations (5a) and equation (5b), the area moment of inertia of total uncracked portion $A_0(t)$about Y and Z axes is written as,

$$I_Y^{A_0}(t) = I_y^{A_0}(t) - A_0(t) y_C(t)^2 \tag{8a}$$

$$I_Z^{A_0}(t) = I_z^{A_0}(t) - A_0(t) z_C(t)^2 \tag{8b}$$

where, $y_0(t)$ and $z_0(t)$ are the time-dependent coordinates of the centroid C.

The preceding equations (8a) and (8b) give an approximate solution for the area moment of inertia when solved individually for $I_Y^{A_0}(t)$ and $I_Z^{A_0}(t)$ through Fourier series expansion.

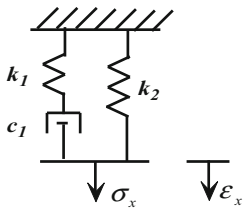

Figure 2. Standard 3- Element Model.

$$I_Y^{A_0}(t) = I - (I - I_Z^{A'}) f_1(t) \tag{9a}$$

$$I_Z^{A_0}(t) = I + (I - I_Y^{A'}) f_1(t) - (2I - I_Y^{A'} - I_Z^{A'}) f_2(t) \tag{9b}$$

where, $f_1(t) = \left(\cos\left(\frac{1}{2}\Omega t\right)\right)^m$; $f_2(t) = \frac{1}{\pi}\left(-\frac{\theta_1+\theta_2}{2} + \frac{2}{(\theta_2-\theta_1)} \sum_{i=1}^{p} \frac{\cos(i\theta_2)-\cos(i\theta_1)}{i^2}\cos(i\Omega t)\right)$

This time-dependent moment of inertia is used in the finite element matrix, which reflects the breathing crack behavior. The stiffness matrix $[\mathbf{K_B^c}]$of the breathing crack element of the rotor shaft is written as,

$$[K_B^c] = \frac{E}{l^3}\begin{bmatrix} 12I_Y^{A_0}(t) & 6lI_Y^{A_0}(t) & 0 & 0 & -12lI_Y^{A_0}(t) & 6lI_Y^{A_0}(t) & 0 & 0 \\ 6lI_Y^{A_0}(t) & 4l^2I_Y^{A_0}(t) & 0 & 0 & -6lI_Y^{A_0}(t) & 2l^2I_Y^{A_0}(t) & 0 & 0 \\ 0 & 0 & 12I_Z^{A_0}(t) & 6lI_Z^{A_0}(t) & 0 & 0 & -12I_Z^{A_0}(t) & 6lI_Z^{A_0}(t) \\ 0 & 0 & 6lI_Z^{A_0}(t) & 4l^2I_Y^{A_0}(t) & 0 & 0 & -6lI_Y^{A_0}(t) & 2l^2I_Y^{A_0}(t) \\ -12lI_Y^{A_0}(t) & -6lI_Y^{A_0}(t) & 0 & 0 & 12I_Y^{A_0}(t) & -6lI_Y^{A_0}(t) & 0 & 0 \\ 6lI_Y^{A_0}(t) & 2l^2I_Y^{A_0}(t) & 0 & 0 & -6lI_Y^{A_0}(t) & 4l^2I_Z^{A_0}(t) & 0 & 0 \\ 0 & 0 & -12I_Y^{A_0}(t) & -6lI_Y^{A_0}(t) & 0 & 0 & 12I_Y^{A_0}(t) & 6lI_Y^{A_0}(t) \\ 0 & 0 & 6lI_Z^{A_0}(t) & 2l^2I_Z^{A_0}(t) & 0 & 0 & 6lI_Z^{A_0}(t) & 4l^2I_Z^{A_0}(t) \end{bmatrix} \tag{10a}$$

The accurate solution of $I_Y^{A_0}(t)$ and $I_Z^{A_0}(t)$ is derived by carrying out the Fourier series expansion over $I_Y^{A_0}(t) + I_Z^{A_0}(t)$ which actually matches the trend of time-dependent area $A_0(t)$ unlike when solved individually (Al-Shudeifat and Butcher [12]). This accurate relationship for $I_Y^{A_0}(t)$ and $I_Z^{A_0}(t)$ is derived to be,

Following this stiffness matrix, the expression of circulatory stiffness matrix $[\mathbf{K_C^c}]$ of the cracked element due to internal damping is given as,

$$[K_C^c] = \frac{E}{l^3}\begin{bmatrix} 0 & 0 & 12I_Y^{A_0}(t) & -6lI_Y^{A_0}(t) & 0 & 0 & -12lI_Y^{A_0}(t) & -6lI_Y^{A_0}(t) \\ 0 & 0 & 6lI_Y^{A_0}(t) & -4l^2I_Y^{A_0}(t) & 0 & 0 & -6lI_Y^{A_0}(t) & -2l^2I_Y^{A_0}(t) \\ 12I_Z^{A_0}(t) & 6lI_Z^{A_0}(t) & 0 & 0 & 12I_Z^{A_0}(t) & -6lI_Z^{A_0}(t) & 0 & 0 \\ -6lI_Z^{A_0}(t) & -4l^2I_Y^{A_0}(t) & 0 & 0 & -6lI_Y^{A_0}(t) & 2l^2I_Y^{A_0}(t) & 0 & 0 \\ 0 & 0 & 12lI_Y^{A_0}(t) & -6lI_Y^{A_0}(t) & 0 & 0 & 12I_Y^{A_0}(t) & 6lI_Y^{A_0}(t) \\ 0 & 0 & -6lI_Y^{A_0}(t) & 2l^2I_Y^{A_0}(t) & 0 & 0 & -6lI_Y^{A_0}(t) & -4l^2I_Z^{A_0}(t) \\ -12I_Y^{A_0}(t) & -6lI_Y^{A_0}(t) & 0 & 0 & 12I_Y^{A_0}(t) & 6lI_Y^{A_0}(t) & 0 & 0 \\ -6lI_Z^{A_0}(t) & -2l^2I_Z^{A_0}(t) & 0 & 0 & -6lI_Z^{A_0}(t) & -4l^2I_Z^{A_0}(t) & 0 & 0 \end{bmatrix} \tag{10b}$$

2.2 *Finite element formulation of viscoelastic shaft*

For any viscoelastic material, the generic form of constitutive relation is represented by,

$$\sigma = E()\varepsilon \tag{11}$$

$E()$ in the above equation stands for the modulus operator with polynomials in numerator and denominator being a function of D i.e., a time differential operator. The order of polynomials depends on the number of spring and dashpot considered to establish the viscoelastic law of the material.

Figure 2 represents a 3-element rheological model whose modulus operator is given in equation (12) where, a_0, a_1, b_0, b_1 are the operator parameters presenting viscoelastic material properties.

$$E() = \frac{a_0 + a_1 \mathrm{D}}{b_0 + b_1 \mathrm{D}} \tag{12}$$

where, $a_0 = k_2$, $a_1 = c_1 + \frac{k_2 c_1}{k_1}$, $b_0 = 1$, $b_1 = \frac{c_1}{k_1}$

A 3 element model is considered for viscoelastic material and the equation of motion for the propeller shaft system mounted on journal bearings is represented as [7],

$$[\mathbf{A_0}]\{\mathbf{q}\} + [\mathbf{A_1}]\{\dot{\mathbf{q}}\} + [\mathbf{A_2}]\{\ddot{\mathbf{q}}\} + [\mathbf{A_3}]\{\dddot{\mathbf{q}}\} = [\mathbf{B}]\{\sqcap\} \tag{13}$$

The preceding finite element formulation is a higher-order form and various coefficients of this equation are given as,

$$\begin{aligned}
[\mathbf{A_0}] &= (a_0)[\mathbf{K_B}] + \Omega(a_1)[\mathbf{K_C}] + \left[\mathbf{K_{brg}}\right] \\
[\mathbf{A_1}] &= (b_0)[\mathbf{G}] + (a_1)[\mathbf{K_B}] + \left[\mathbf{C_{brg}}\right] \\
[\mathbf{A_2}] &= (b_0)[\mathbf{M}] + (b_1)[\mathbf{G}] \\
[\mathbf{A_3}] &= (b_1)[\mathbf{M}] \\
[\mathbf{B}] &= (b_0 + b_1 D)[\mathbf{P}]
\end{aligned}$$

where, $\{\mathbf{q}\}$denotes the nodal degrees of freedom and $[\mathbf{M}]$, $[\mathbf{G}]$, $[\mathbf{K_B}]$, $[\mathbf{K_C}]$, $\left[\mathbf{K_{brg}}\right]$, $\left[\mathbf{C_{brg}}\right]$ are the mass matrix, gyroscopic matrix, bending stiffness matrix, circulatory stiffness matrix, bearing stiffness and bearing damping matrix respectively.

From modelling point of view, one of the basic steps involved in finite element analysis procedure is the assembling of elemental matrices to obtain global matrices. The elemental matrices in equation (13) differ for crack element due to the varying stiffness as represented in section 2.1. Initially, the globalization of the finite element matrices is carried out in the usual manner for the intact elements. Later, according to nodal connectivity, the cracked element is assembled considering the expression of $\left[\mathbf{K_B^c}\right]$ and $\left[\mathbf{K_C^c}\right]$(Eq. (10)), and the final global matrices of the entire continuum are formed.

Further, the higher-order equation of motion is transformed into the state-space format [25] in order to perform a simplified eigen analysis of the system.

$$\{\dot{\S}\} = [\mathcal{A}]\{\S\} + [\mathcal{B}]\{\sqcap\} \tag{14a}$$

$$\{\dagger\} = [\mathcal{C}]\{\S\} + [\mathcal{D}]\{\sqcap\} \tag{14b}$$

where,

$$[\mathcal{A}] = \begin{bmatrix} [\mathbf{0}] & [\mathbf{I}] & [\mathbf{0}] \\ [\mathbf{0}] & [\mathbf{0}] & [\mathbf{I}] \\ \left[-\mathbf{A_3^{-1}A_0}\right] & \left[-\mathbf{A_3^{-1}A_1}\right] & \left[-\mathbf{A_3^{-1}A_2}\right] \end{bmatrix}$$

$$[\mathcal{B}] = \begin{bmatrix} [\mathbf{0}] \\ [\mathbf{0}] \\ [\mathcal{B}] \end{bmatrix}, \{\S\} = \begin{Bmatrix} \mathbf{q} \\ \dot{\mathbf{q}} \\ \ddot{\mathbf{q}} \end{Bmatrix}$$

where, $[\mathcal{A}]$, $[\mathcal{B}]$, $[\mathcal{C}]$and $[\mathcal{D}]$ are the system state matrix, input matrix, output matrix and direct transmission matrix respectively. $\{\S\}$ is the state vector and $\{\mathbf{u}\}$is the force vector with its appropriate nodal position decided by matrix $[\mathbf{P}]$. The analysis of the system matrix $[\mathcal{A}]$ using the predefined MATLAB function 'condeig' yields the eigen values of the rotating shaft system with crack.

3. Results and discussion

3.1 *Validation*

The finite element model of an undamped rotor-disk system mounted on journal bearings at its two ends mentioned in Al-Shudeifat and Butcher [12] is taken first to validate the present formulation using Matlab. Figure 3 represents the rotor model whose length is discretized in 18 finite elements with two disks mounted on the shaft length considering a mass unbalance on the rigid disk 2. The rotor system and disk details are mentioned in tables 1 and 2, respectively.

On formulating the time-dependent breathing crack stiffness matrix for a cracked element using new breathing functions, the global system matrices are developed for cracked rotor and the undamped system equation of motion is established. In order to validate the code, unbalance response of the cracked shaft system due to unbalance mass in the second disc from the left end is plotted in Figure 4 and matched with results obtained by Al-Shudeifat and

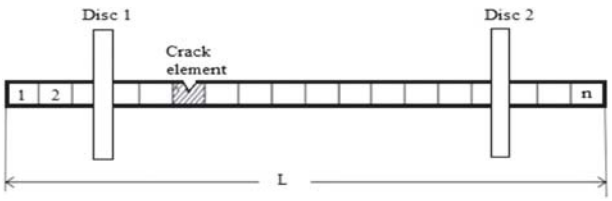

Figure 3. Discretized rotor disk system (Al-Shudeifat and Butcher [12]).

Table 1. Shaft data.

Model parameters	Value
Length of the shaft, L	0.724 m
Radius of the rotor, r	15.88 mm
Density of rotor, ρ	7800 kg/m^3
Modulus of elasticity, E	2.1e11 N/m^2
Bearing stiffness, k_{xx}, k_{yy}	7e7N/m
Bearing Damping, c_{xx}, c_{yy}	5e2N s/m

Table 2. Disk data.

Disk parameters	Value
Inner Radius of disk, r_i	15.88 mm
Outer Radius of disk, r_o	0.0762 m
Disk Density, ρ_d	2700 kg/m^3
Disk mass, M_d	0.571 kg
Mass unbalance, $M_e d$	10e-6 kg m

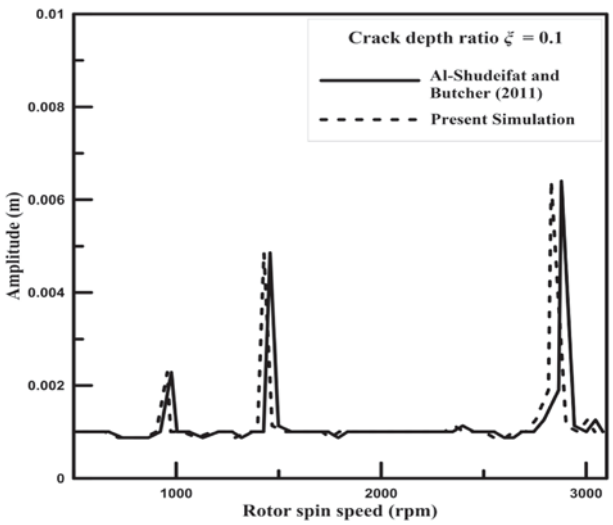

Figure 4. Unbalance response validation.

Butcher [12] at a non-dimension crack depth ratio of $\xi = \frac{h}{r} = 0.1$.

3.2 *Problem definition*

A hollow propeller shaft system represented in figure 5 referred from Zhang *et al* [26] is considered here for studying its dynamic characteristics. The geometrical parameters of the steel propeller shaft tabulated in table 3 are taken close to the constraints recognized from the realistic technical application. Both propeller and coupling mounted at two ends of the shaft continuum are assumed as rigid discs of mild steel whose mobility is similar to the shaft mobility at its location. These disc parameters are mentioned in table 4. The whole shaft is braced by 3 identical journal bearings at different locations, hence dividing the shaft into 4 sections with distances L_1, L_2, L_3 and L_4. The journal bearing parameters are given in table 5.

Before going to discuss the dynamic analysis, a convergence test is conducted in order to deduce the total number of elements. The shaft length is discretized into a hundred Euler-Bernoulli beam elements (or 101 nodes) where each element having 2 nodes at its end and four degrees of freedom per node i.e., 2-translational and 2-rotational. For proper placement of bearings at its defined locations, each of the 4 shaft sections is divided into the required number of finite elements as given in table 6 which ultimately sums up to a hundred elements.

3.2a *Dynamic analysis*: The Finite element based derived equation of motion is used for dynamic analysis of a cracked propeller shaft. The dynamic performances of the cracked shaft are evaluated by comparing it with the similar uncracked shaft. The non-dimensional crack length $\xi = 0.5$ is considered at element 3 from the left end in section 1 of the shaft continuum. Both eigen analysis and frequency response analysis are performed here.

3.2.1a *Decay rate plot*: The plot in figure 6 depicts the relation between maximum real parts of eigenvalue with respect to the rotational speed of the shaft. The graph helps to determine the stability limit of spin speed (SLS) of the system at a point where the line cuts the zero line. The region below the zero line stands for a stable zone while above zero line indicates an unstable zone. The plot clearly represents a reduction in the SLS of the propeller shaft with the crack condition when compared with the intact shaft system as a result of reduced stiffness.

3.2.1b. *Campbell diagram*: Campbell diagram is a plot using the imaginary component of the system eigenvalues representing the whirl frequency varying with spin speed of the rotor. Figure 7 demonstrates the first bending mode of the cracked as well as the uncracked shaft along with the 45° synchronous whirl line (SWL). The two sets of diverging lines indicate the 1st forward and backward whirling of the cracked and the uncracked rotating shaft. The point at which the SWL cuts the diverging lines designates the 1st forward and backward natural frequencies of the respective shaft system. It is evident from the plot that the presence of crack decreases the forward and backward whirl frequencies due to reduced system stiffness.

3.2.1c *Modal damping factor*: Modal damping factor (MDF) is defined as the negative ratio of the real part of the eigenvalues to its corresponding imaginary part. Figure 8 plots the values of MDF with varying spin speed and compare the same between the cracked and intact propeller shaft system. In this figure, the region above the zero line stands for a stable zone while below zero line denotes an

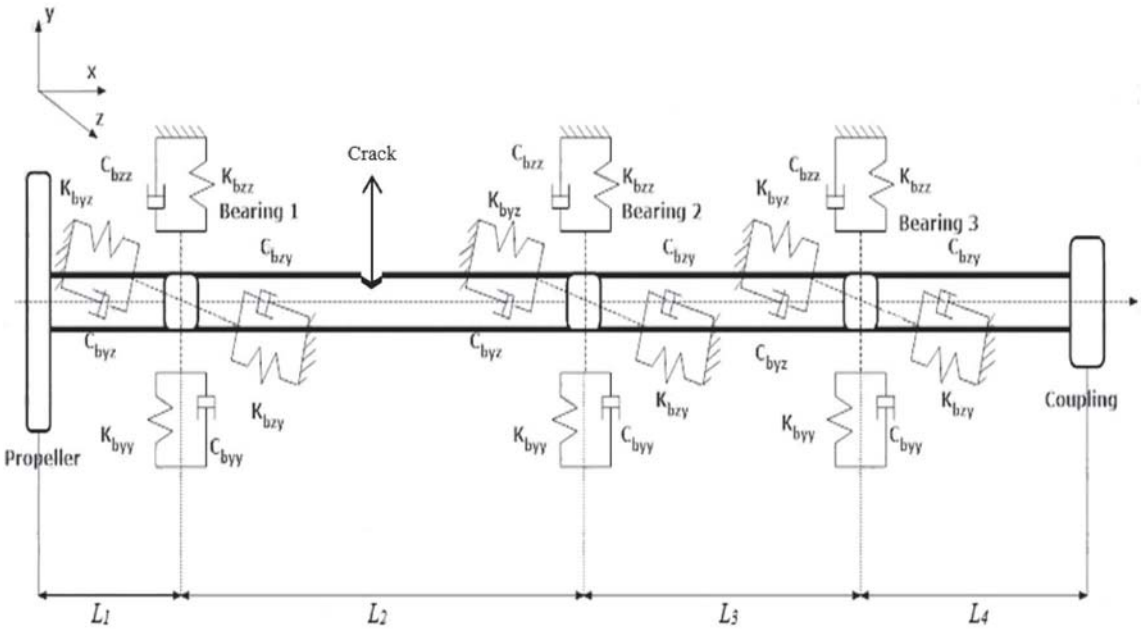

Figure 5. Propeller shaft system.

Table 3. Shaft data.

	Viscoelastic parameters				Radius (m)	
Density (Kg/m^3)	a_0	b_0	a_1	b_1	Inner Radius	Outer Radius
7800	2.1e+11	1	7.51e+5	1.475e-9	0.075	0.14

Table 4. Disc data.

Discs	Material	Mass (kg)	Polar moment of Inertia (kg m^2)	Disc node
Propeller	Mild Steel	7000	3100	1
Coupling	Mild Steel	1500	350	101

Table 5. Bearing data.

Bearing properties	Stiffness	Damping
Plane yy	5.5e8	5e2
Plane zz	5.5e8	7e2

unstable zone. Hence, the point at which the changing MDF value with respect to the spin speed cuts the zero line in the figure signifies the SLS of the system. A significant decrement in the SLS is observed in the cracked rotating shaft (1590 rpm) when compared with that of the uncracked shaft (1880 rpm).

3.2.1d *Unbalance response*: Figure 9 plots the unbalance response, which is a plot between response amplitude due to the unbalance mass of the propeller disc and input spin speed. Unbalance response is measured at propeller disc marked as node 1. The plot compares the frequency response of the intact and cracked shaft. The reduction in natural frequency and increased response of the cracked shaft clearly indicates the effect of the crack in the propeller shaft system when compared with the intact shaft.

3.2.2 *Parametric study of the cracked propeller shaft*: Parametric studies considering different cracked depth ratios and crack locations are carried out to understand the dynamic behavior of the long propeller shaft system. For this, the whole shaft length is divided into four sections

Table 6. Shaft continuum sections.

Shaft section length notation	Shaft length (m)	Number of elements
L_1	0.85	4
L_2	9.65	49
L_3	7.5	37
L_4	2.0	10

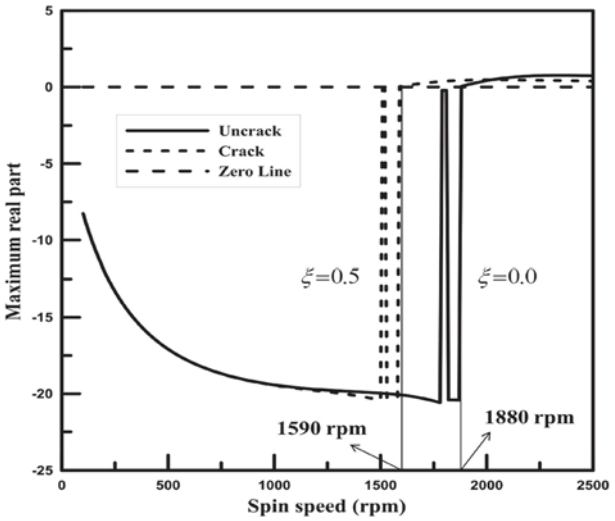

Figure 6. Decay rate plot, uncracked vs. cracked propeller shaft.

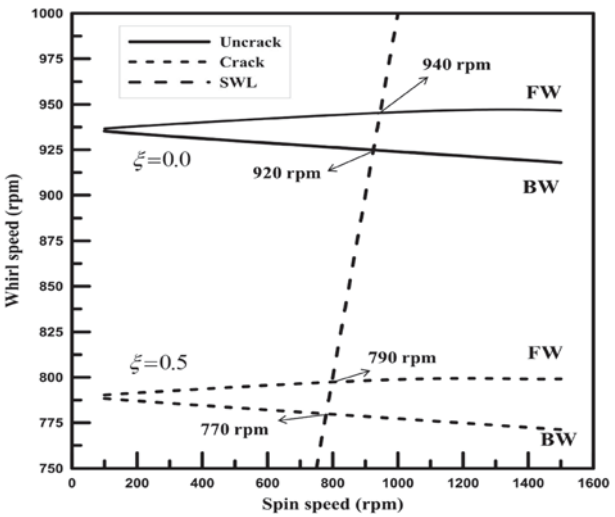

Figure 7. Campbell diagram, uncracked vs. cracked propeller shaft.

between the Propeller disc (P_d), Bearing 1 (B_1), Bearing 2 (B_2), Bearing 3 (B_3) and Coupling disc (C_d). Figures 10 and 11 show the variation of non-dimensional stability limit of spin speed (SLS*) and non-dimensional first natural

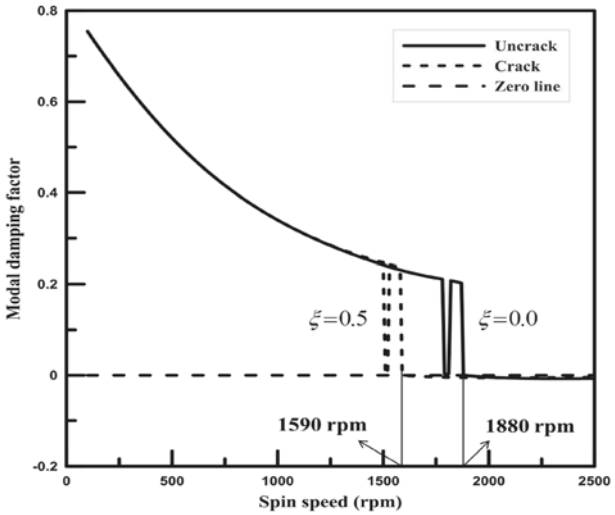

Figure 8. Modal damping factor, uncracked vs. cracked propeller shaft.

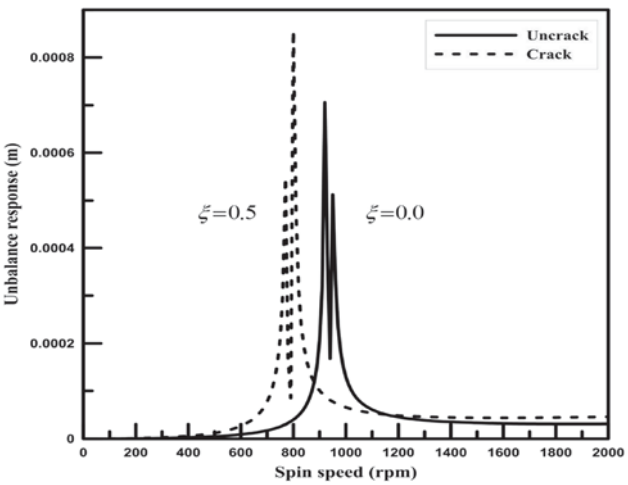

Figure 9. Mass unbalance response, uncracked vs. cracked propeller shaft.

frequency (FNF*) at different crack locations. The non-dimensionalisation of these parameters (SLS*, FNF*) is done by dividing the parametric values of the cracked system with the respective values of intact system. Depending upon the magnitude of bending stress at different locations of shaft, similar variation trend of SLS* and FNF* are also observed. As the two overhung sections of the shaft have maximum bending moment at the support ends, a sudden drop in SLS* and FNF* is observed when the crack element location is close to the support end of these cantilever section. Their values again gradually increase for any particular crack depth ratio as the crack element location shifts towards the free ends of either of the sections. However, with an increase in crack depth ratio $\xi = 0.1, 0.3, 0.5$, the SLS* and FNF* are observed to be decreasing at any particular crack location as the system

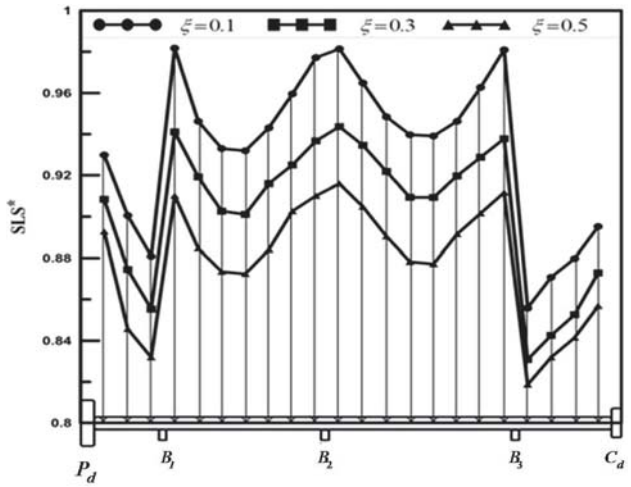

Figure 10. Non-dimensional stability limit of spin speed vs. crack location for different crack depth ratio.

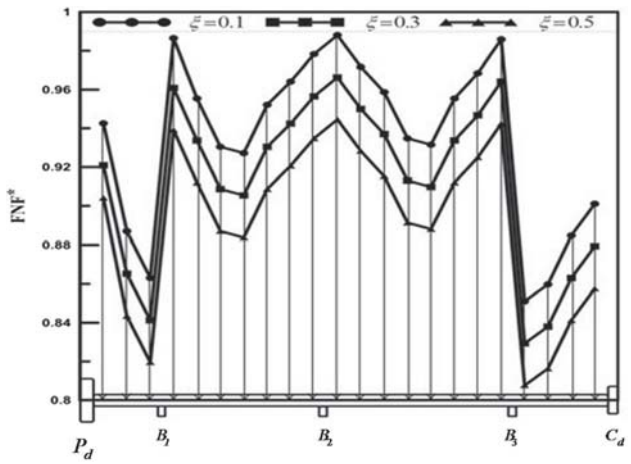

Figure 11. Non-dimensional first natural frequency vs. crack location for different crack depth ratio.

losses its stiffness with gradual increase in the crack depth ratio.

4. Summary and conclusions

The present study focuses on the dynamic analysis of viscoelastic rotor shaft with transverse breathing cracked. For this, a real problem of propeller shaft braced by journal bearings is considered. Speed-dependent area moment of inertia is taken for breathing behaviour that introduces the time-dependent stiffness matrix of the breathing crack element. The global stiffness matrix is obtained by assembling the stiffness matrix of the cracked element with that of the intact elements following the finite element procedure. The higher-order finite element equation of motion of a viscoelastic propeller shaft system is developed through the operator based method. The comparative study is carried out based on different dynamic parameters like whirl frequency, modal damping factor and stability limit of spin speed, which are obtained from eigen analysis of the higher-order model. The presence of crack reduces the natural frequencies and enhances the unbalance response as a result of reduced stiffness of the cracked shaft. Further, the variation in SLS and FNF are studied on varying parameters i.e., crack locations and crack depth. Crack present in different sections of the propeller shaft gives a varying eigen analysis result for the same crack depth ratio. Additionally, for any particular crack position in the shaft, the eigen values are observed to be decreasing in nature as the crack element stiffness decreases with an increase in crack depth.

List of symbols

A	Cross-sectional area of rotor
A_c	Area of the cracked segment
A'	Area of the uncracked segment
O	Centre of the whole cross-section
C	Centroid of the uncracked portion
c	Distance between O and C
h	Depth of the crack
r	Radius of the shaft cross-section
θ	Angle made by the crack segment at the centre
θ_1	Angle at which the crack starts to close
θ_2	Angle at which the crack is fully closed
$A''(t)$	Time-varying area of the closed crack segment
I	Area moment of inertia of the whole cross-section
$I_y^{A'}$	Area moment of inertia of uncracked segment about y axis
$I_z^{A'}$	Area moment of inertia of uncracked segment about z axis
$I_y^{A_c}$	Area moment of inertia of cracked segment about y axis
$I_z^{A_c}$	Area moment of inertia of cracked segment about z axis
$A''(t)$	Time dependent area of the cracked segment
$I_y^{A'}(t)$	Time dependent area of the cracked segment about y axis
$I_z^{A'}(t)$	Time dependent area of the cracked segment about z axis
$A_0(t)$	Time dependent area of the uncracked segment
$I_y^{A_0}(t)$	Time dependent area of the uncracked segment about y axis
$I_y^{A_0}(t)$	Time dependent area of the uncracked segment about y axis
$[K_B^c]$	Stiffness matrix of the breathing crack element

$[K_C^c]$	Circulatory Stiffness matrix of the breathing crack element
σ	Stress
ε	Strain
$E()$	Modulus operator
a_0, a_1, b_0, b_1	Viscoelastic operator parameters
$\{\mathbf{q}\}$	Nodal degrees of freedom
$\{\mathbf{u}\}$	Force vector
$[\mathbf{M}]$	Mass matrix
$[\mathbf{G}]$	Gyroscopic matrix
$[\mathbf{K_B}]$	Bending stiffness matrix
$[\mathbf{K_C}]$	Circulatory stiffness matrix
$[\mathbf{K_{brg}}]$	Bearing stiffness matrix
$[\mathbf{C_{brg}}]$	Bearing damping matrix
$[\mathcal{A}]$	System state matrix
$[\mathcal{B}]$	Input matrix
$[\mathcal{C}]$	Output matrix
$[\mathcal{D}]$	Direct transmission matrix
ξ	Non-dimension crack depth ratio

References

[1] Rao J S 1991 *Rotor Dynamics*. Wiley, New York

[2] Chouksey M, Dutt J K and Modak S V 2012 Modal analysis of rotor shaft system under the influence of rotor-shaft material damping and fluid film forces. *Mechanism and Machine Theory* 48: 81-93

[3] Bland D R 1960 *Linear Viscoelasticity*. Pergamon Press, Oxford

[4] Christensen R M 1982 *Theory of Viscoelasticity: an Introduction*. Academic Press, New York

[5] Shames I and Cozzarelli F 1992 *Elastic and inelastic stress analysis*. Prentice-Hall. Inc. Englewood Cliffs, NJ

[6] Dutt J K and Roy H 2011 Viscoelastic modelling of rotor—shaft systems using an operator-based approach. In: *Proceedings of the Institution of Mechanical Engineers, Journal of Mechanical Engineering Science* 225(1): 73-87

[7] Roy H and Chandraker S 2017 Dynamic study of viscoelastic rotor: Modal analysis of higher order model considering various asymmetries. *Mechanism and Machine Theory*109: 65-77

[8] Schmied J and Kramer E 1984 Vibration behaviour of a rotor with a cross-sectional crack. In: *Int. conf. Vibr. Rot. Mach. Pap. Int. Conf. Heslidtion*. 183:11-13

[9] Jun O S, Eun H J, Earmme Y Y and Lee CW 1992 Modelling and vibration analysis of a simple rotor with a breathing crack. *Journal of Sound and Vibration* 155(2): 273-290

[10] Sinou J J and Lees A W 2005 The influence of cracks in rotating shafts. *Journal of Sound and Vibration* 285(4-5): 1015-1037

[11] Georgantzinos S K and Anifantis N K 2008 An insight into the breathing mechanism of a crack in a rotating shaft. *Journal of Sound and Vibration* 318(1-2): 279-295

[12] Al-Shudeifat M A and Butcher E A 2011 New breathing functions for the transverse breathing crack of the cracked rotor system: approach for critical and subcritical harmonic analysis. *Journal of Sound and Vibration* 330(3): 526-54

[13] Han Q and Chu F 2012 Parametric instability of a rotor-bearing system with two breathing transverse cracks. *European Journal of Mechanics-A/Solids*. 36: 180-190

[14] Guo C, Al-Shudeifat M A, Yan J, Bergman L A, McFarland D M and Butcher E A 2013a Stability analysis for transverse breathing cracks in rotor systems. *European Journal of Mechanics-A/Solids*. 42: 27-34

[15] Guo C, Al-Shudeifat M A, Yan J, Bergman L A, McFarland D M and Butcher E A 2013b Application of empirical mode decomposition to a Jeffcott rotor with a breathing crack. *Journal of Sound and Vibration* 332(16): 3881-3892

[16] Peng H, He Q and Zhen Y 2015 Stability analysis of a breathing cracked rotor with imposed mass eccentricity. *Shock and Vibration,* Article ID 453216: 1-17

[17] Mobarak H M, Wu H, Spagnol J P and Xiao K 2018 New crack breathing mechanism under the influence of unbalance force. *Archive of Applied Mechanics* 88(3): 341-372

[18] Wang S, Bi C, Li J and Zheng C 2019Parametric instability of anisotropic rotor-bearing systems with a transverse crack. *Journal of Sound and Vibration* 443: 253-269

[19] Sinou J J and Lees A W 2007 A non-linear study of a cracked rotor. *European Journal of Mechanics-A/Solids*. 26(1): 152-170

[20] Chen C and Dai L (2007) Bifurcation and chaotic response of a cracked rotor system with viscoelastic supports. *Nonlinear Dynamics* 50(3):483–509

[21] Bachschmid N, Pennacchi P and Tanzi E 2008 Some remarks on breathing mechanism, on non-linear effects and on slant and helicoidal cracks. *Mechanical Systems and Signal Processing* 22(4): 879-904

[22] El-Arem S and Nguyen Q S 2012 Nonlinear dynamics of a rotating shaft with a breathing crack. *Annals of Solid and Structural Mechanics 3*(1-2):1-14

[23] Chen X 2016 Nonlinear responses analysis caused by slant crack in a rotor-bearing system. *Journal of Vibroengineering 18*(7): 4369-4387

[24] Pilkey W D 2002 *Analysis and design of elastic beams: Computational methods*. John Wiley & Sons

[25] Meirovitch L 1975 *Elements of vibration analysis*. McGraw-Hill Science, Engineering & Mathematics

[26] Zhang Z, Zhang Z, Huang X and Hua H 2014 Stability and transient dynamics of a propeller–shaft system as induced by nonlinear friction acting on bearing–shaft contact interface. *Journal of Sound and Vibration* 333(12):2608-2630